# Periodic Nanowire Array at the Crystal Interface

**Atsutomo Nakamura,[†,*] Teruyasu Mizoguchi,[‡] Katsuyuki Matsunaga,[†,§] Takahisa Yamamoto,[§,⊥] Naoya Shibata,[∥] and Yuichi Ikuhara[§,∥,¶]**

[†]Department of Materials Science and Engineering, Nagoya University, Furo-cho, Chikusa-ku, Nagoya, 464-8603 Japan, [‡]Institute of Industrial Science, The University of Tokyo, 4-6-1 Komaba, Meguro-ku, Tokyo, 153-8505 Japan, [§]Nanostructures Research Laboratory, Japan Fine Ceramics Center, 2-4-1 Mutsuno, Atsuta-ku, Nagoya, 456-8587 Japan, [⊥]Department of Quantum Engineering, Nagoya University, Furo-cho, Chikusa-ku, Nagoya, 464-8603 Japan, [∥]Institute of Engineering Innovation, The University of Tokyo, 2-11-16 Yayoi, Bunkyo-ku, Tokyo, 113-8686 Japan. [¶]E-mail: ikuhara@sigma.t.u-tokyo.ac.jp.

**ABSTRACT** A dislocation in a crystalline material has dangling bonds at its core and a strong strain field in its vicinity. Consequently, the dislocation attracts solute atoms and forms a so-called Cottrell atmosphere along the dislocation. A crystalline dislocation can be used as a template to produce nanowires by selectively doping foreign atoms along the dislocation. However, control of the configuration, spacing, and density of the formed periodic nanowire array has heretofore been extremely difficult. Here we show a method for fabricating ordered, electrically conductive nanowire arrays using periodic dislocations at crystal interfaces. As a demonstration, we fabricated arrays of titanium nanowires arranged at intervals of either 13 or 90 nm and then confirmed by scanning probe microscopy that they exhibit electrical conductivity inside an insulating aluminum oxide. Significantly, we were able to precisely control nanowire periodicity by the choice of crystal orientation and/or crystal planes at the crystal interface. This simple method for the fabrication of periodic nanowire arrays of highly controlled density should be widely applicable to electrical, magnetic, and optical devices.

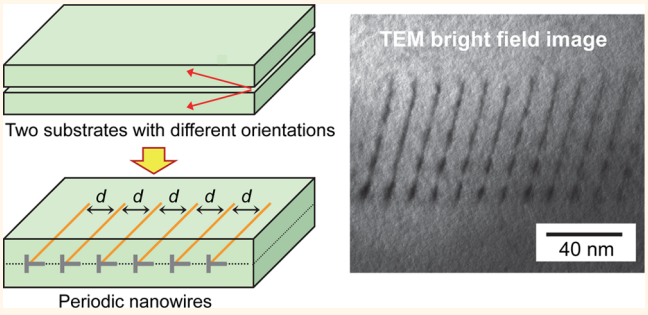


**KEYWORDS:** conductive nanowires · crystal interface · dislocations · grain boundaries · quantum wires

Nanometer-scale materials often exhibit unusual properties that arise from the constraint of extremely limited spaces of specific electronic structures. Recent advancement of nanofabrication techniques has made it possible to fabricate actual nanometer-scale structures. Therefore, low-dimensional nanometer-scale structures, such as one-dimensional quantum dots and two-dimensional quantum wires, are of particular interest.[1−15] A number of techniques for the fabrication of low-dimensional nanometer-scale structures have been proposed. Techniques based on crystal dislocations are promising for the creation of quantum wires, also called nanowires.[5−15] For instance, Ran *et al.*[11] reported that dislocation lines are associated with one-dimensional fermionic excitations in a topological insulator and thus show potential as routes toward fabrication of ideal quantum wires. A crystal dislocation creates a one-dimensional, sub-nanometer-scale lattice discontinuity. The lattice discontinuity then induces the presence of a strain field surrounding the crystal dislocation and of dangling bonds at regular intervals along the lattice discontinuity, modifying the local stoichiometry.[5,6,16,17] Moreover, the core of the dislocation interacts with solute atoms to accommodate its excess elastic energies and dangling bonds. As a result, solute atoms in a crystal tend to segregate to a dislocation, forming a so-called Cottrell atmosphere.[9,18,19] Therefore, by creating a Cottrell atmosphere, we can convert a dislocation into a one-dimensional nanometer-scale structure with unusual functional properties.

To make effective use of such dislocation-based properties, a necessary condition is that we must be able to control dislocation configuration, spacing, and density in a bulk solid. We formerly reported the successful fabrication of conductive nanowire bundles in an insulating sapphire crystal by Cottrell atmosphere design at lattice dislocations.[9,20] In these cited reports, we describe the first successful material design using dislocations,

* Address correspondence to nakamura@numse.nagoya-u.ac.jp.

Received for review May 9, 2013 and accepted June 19, 2013.

**Published online July 05, 2013**
**10.1021/nn4023334**

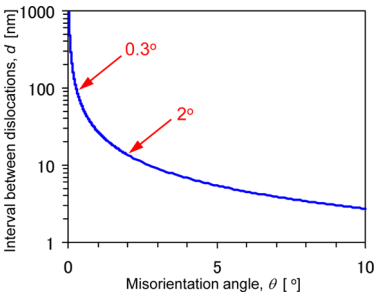


**Figure 1. Plot of the interval between geometrically formed dislocations at a grain boundary as a function of the misorientation angle between the two crystal planes at the boundary. The curve was calculated according to Frank's formula[21] with the assumption that perfect dislocations with a Burgers vector of 1/3 $\langle\bar{1}2\bar{1}0\rangle$ are formed on a $\{\bar{1}2\bar{1}0\}/\langle 10\bar{1}0\rangle$ low-angle tilt grain boundary in aluminum oxide.[26] The angles 0.3 and 2° indicated by arrows correspond to the fabricated nanowires described in this paper.**

which we achieved by the use of high-temperature deformation techniques to generate high-density dislocations and the use of heat treatment to control dislocation directionality. Thus, although unidirectional dislocation bundles were fabricated successfully, the fabrication route was elaborate and demanding.[20] In contrast, Tokumoto *et al.*[14] and Amma *et al.*[15] fabricated functional nanowires using threading dislocations in thin films grown by metal-organic chemical vapor deposition (MOCVD). Their techniques can efficiently fabricate high-density functional nanowires in thin films, with nanowire spacing of less than 100 nm. However, they do not enable sufficient control of nanowire configuration, spacing, or density.

Here we report a novel method for fabricating ordered and controllable conductive nanowire arrays using periodic dislocations formed at the interface of two crystals. We focus on dislocations at low-angle grain boundaries, which is a simple example of a crystal interface, because their configuration, spacing, and density can be controlled easily by the choice of crystal orientation and/or crystal planes at the boundary. If a grain boundary has low-angle misorientation, for example, the periodicity of geometrically formed dislocations at the boundary depends on the misorientation angle between the two crystals that form the boundary. It is well-known that the relationship between the misorientation angle $\theta$ and the interval between grain-boundary dislocations $d$ is given by Frank's formula $\theta = |b|/d$, where $b$ is the Burgers vector of the boundary dislocations.[21]

Figure 1 shows a plot of dislocation interval as a function of misorientation angle according to this formula. The dislocation interval $d$ is simply inversely proportional to the misorientation angle. Thus, we should be able to precisely control the periodicity of the boundary dislocations on a nanometer scale by controlling the misorientation angle during fabrication of a low-angle grain boundary between two single-crystal

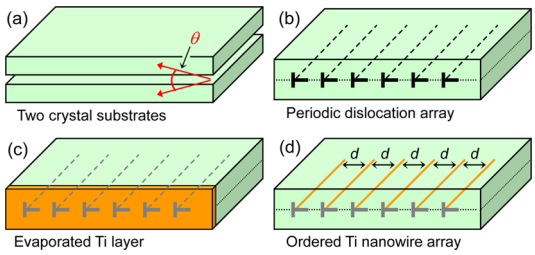


**Figure 2. Fabrication process for the creation of a periodic conductive nanowire at a crystal interface. (a) Two aluminum oxide single-crystal substrates before bonding, each with a slightly different crystal orientation. (b) Fabricated bicrystal after bonding, with periodic dislocations at the grain boundary. (c) Layer of evaporated Ti film on the bicrystal surface. (d) Periodic dislocations modified by Ti to constitute a periodic conductive nanowire.**

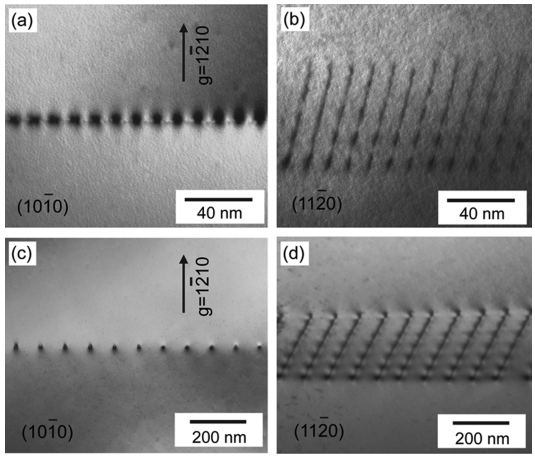


**Figure 3. Typical TEM bright-field images of periodic dislocation arrays at the tilt grain boundaries in the fabricated bicrystals before Ti modification. (a) Image of the 2° tilt grain boundary, observed along the $[10\bar{1}0]$ direction; the periodicity is about 13 nm. (b) Image obtained by tilting the beam direction around [0001] from the state in (a). (c) Image of the 0.3° tilt grain boundary, observed along the $[10\bar{1}0]$ direction; the periodicity is about 90 nm. (d) Image obtained by tilting the beam direction around [0001] from the state in (c). The images suggest that straight, periodic dislocations are present through the interiors of all of the TEM specimens.**

substrates. Because Frank's formula can be realized up to about $\theta = 15°$, the minimum limit of interval $d$ reaches less than 2 nm in theory.

Figure 2 shows our proposed process for fabricating periodic conductive nanowires using low-angle grain boundaries. For the template material, we chose sapphire (aluminum oxide single crystal) because dislocation structures in sapphire have already been well-characterized.[16,17,22−25] Sapphire is one of the most widely used oxide crystals because of its superior properties as a refractory and transparent structural material, optical material, insulator, chemically stable substrate, and much more. We began by preparing two pristine sapphire substrates with slightly different crystal orientations (Figure 2a). The two substrates were joined by diffusion bonding in air at 1500 °C for 10 h, resulting in a fabricated bicrystal with periodic dislocations

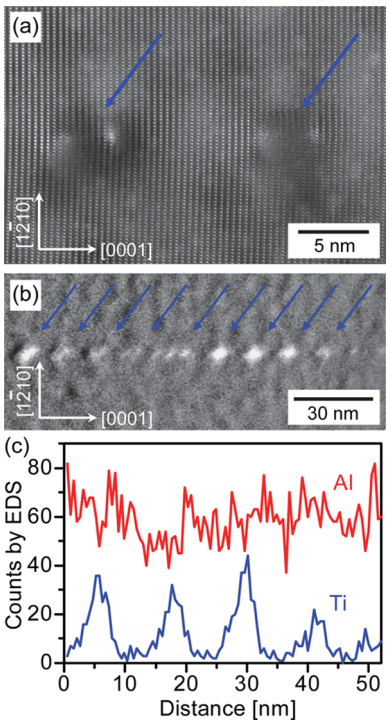


**Figure 4. Periodic dislocation arrays after Ti modification. (a) Typical HRTEM image around the dislocations at the 2° grain boundary. The core structure of each nanowire is obscured. (b) Energy-filtered TEM image derived from an energy loss of 435−485 eV, which includes loss by the Ti $L_{2,3}$ edges. Blue arrows in (a) and (b) indicate individual nanowires. (c) EDS compositional profile of Al and Ti. It is evident that the periodic dislocations modified by Ti result in periodic Ti-enriched nanowires.**

at the grain boundary (Figure 2b). Such a fabricated bicrystal with low misorientation can be treated as a single crystal with an ordered, periodic dislocation array inside. Ti was then evaporated on the bicrystal surface (Figure 2c). Finally, the bicrystal with evaporated Ti was heat-treated at 1400 °C for 2 h in a reducing atmosphere of 95% Ar + 5% $H_2$, resulting in periodic dislocations modified by Ti (Figure 2d). Thus, we succeeded in fabricating periodic nanowires inside a sapphire crystal. The crystallographic orientation of the grain boundary corresponds to a $\{\bar{1}2\bar{1}0\}/\langle 10\bar{1}0\rangle$ low-angle tilt grain boundary, where the Burgers vector of formed dislocations is 1/3 $\langle\bar{1}2\bar{1}0\rangle$. Additional details of the crystallographic characteristics of boundary dislocations are described elsewhere.[26]

## RESULTS AND DISCUSSION

Figure 3a,b shows transmission electron microscopy (TEM) bright-field images of a fabricated bicrystal with a misorientation angle of 2°, before Ti modification of the grain-boundary dislocations. The image in Figure 3a was taken parallel to the dislocation lines, while that in Figure 3b was obtained by tilting the beam direction around [0001] from Figure 3a. In Figure 3a, strain fields due to individual dislocations appear as small dots; in contrast, in Figure 3b, aligned unidirectional dislocations are clearly evident. Thus, the periodic dot-like contrasts in Figure 3a correspond to straight dislocations that penetrate the TEM specimen. An ordered, periodic dislocation array results with a periodicity of about 13 nm. This periodicity is

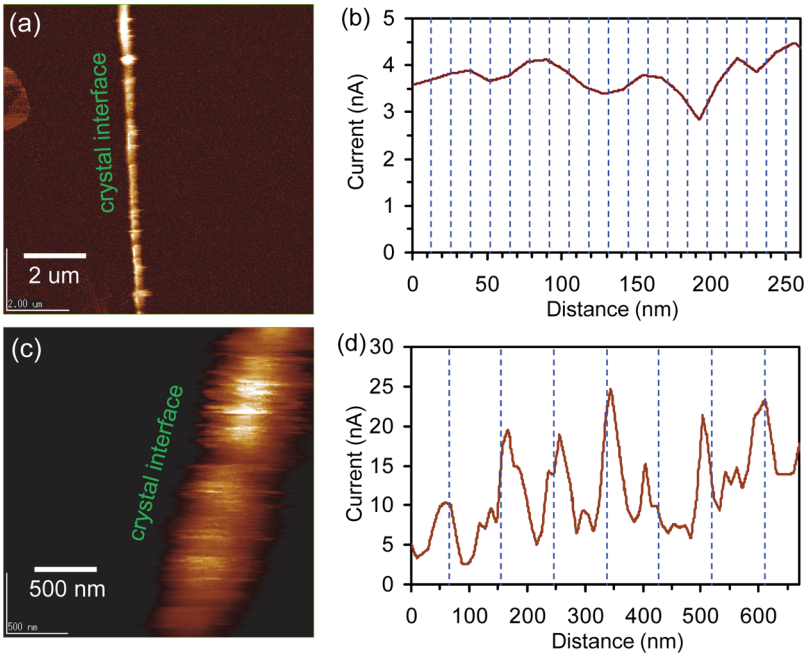


**Figure 5. Conductive AFM images (a,c) and plots of periodic nanowire conductivity (b,d) at two types of grain boundaries; those with 2° (a,b) and 0.3° (c,d) misorientations. The plots of periodic nanowire conductivity are shown as a function of distance in the [0001] direction, which is parallel to the boundaries and perpendicular to the nanowires. The measurements are performed by SPM in contact-current mode with an applied voltage of 100 V at room temperature in air. In the both plots, the spacing of the blue dotted lines corresponds to the nanowire periodicity. The observed peak interval in (d) corresponds to the nanowire periodicity, suggesting that each nanowire contributes to the electric conduction.**

consistent with the value of $d$ obtained from Frank's formula with a misorientation angle of 2° and $b$ = 0.476 nm. To demonstrate an ordered, periodic dislocation array with a different interval, we took images of another fabricated bicrystal with a different misorientation angle, 0.3°, as shown in Figure 3c,d. As above, the image in Figure 3d was obtained by tilting the beam direction from Figure 3c. The interval between dislocations is about 90 nm, which is consistent with a misorientation of 0.3° at the $\{\bar{1}2\bar{1}0\}/\langle 10\bar{1}0\rangle$ low-angle tilt grain boundary.

Figure 4a shows a typical high-resolution TEM (HRTEM) image around the dislocations at the 2° grain boundary, after Ti modification of the grain-boundary dislocations. The core structure of each nanowire is obscured, although the core of the original dislocation is not obscured and was characterized previously.[16,26] Figure 4b shows an energy-filtered TEM image made with Ti $L_{2,3}$ edges at 435−485 eV. Ti is clearly present along the periodic dislocations at the 2° grain boundary. Brightness intensity differs for different nanowires, presumably because the incident electron beam is slightly inclined to the line direction of the nanowires because of the distortion of the TEM specimen. Figure 4c shows EDS compositional profiles of Al and Ti along the periodic dislocation array. Ti concentration increases significantly at the positions of periodic dislocations with diameters of about 5 nm. Thus, periodic dislocations modified by Ti clearly result in periodic nanowires. In addition, by electron beam scattering, we note that Ti profiles obtained by EDS broaden.

Figure 5 shows conductive atomic force microscopy (AFM) images taken from around two types of grain boundaries with different misorientation in (a) and (c), and plots of periodic nanowire conductivity in (b) and (d). Here, (a) and (b) are obtained from a 2° grain boundary, while (c) and (d) are from a 0.3° grain boundary. The measurements are performed by a scanning probe microscope (SPM) in contact-current mode with an applied voltage of 100 V at room temperature in air. The grain boundaries appear as a bright band on the conductive AFM images as can be seen in (a) and (c). The horizontal axes in the both plots of (b) and (d) correspond to the distance in the [0001] direction, which is parallel to the boundaries and perpendicular to individual nanowires. On the other hand, the vertical axes correspond to the electric current that flow in the $[10\bar{1}0]$ direction, which is parallel to the nanowires. Note that the conductivity of bulk sapphire is known to be negligibly small. For nanowires at a 2° grain boundary, we were unable to discriminate conduction by individual nanowires (Figure 5b) because the nanowire interval was very small for the SPM probe to resolve individual wires. For a separation distance of 13 nm and nanowire diameter of 5 nm, the nonconduction region is only 8 nm wide, which is less than the average radius of 10 nm of an ideal probe. In addition, a probe would be damaged by contact

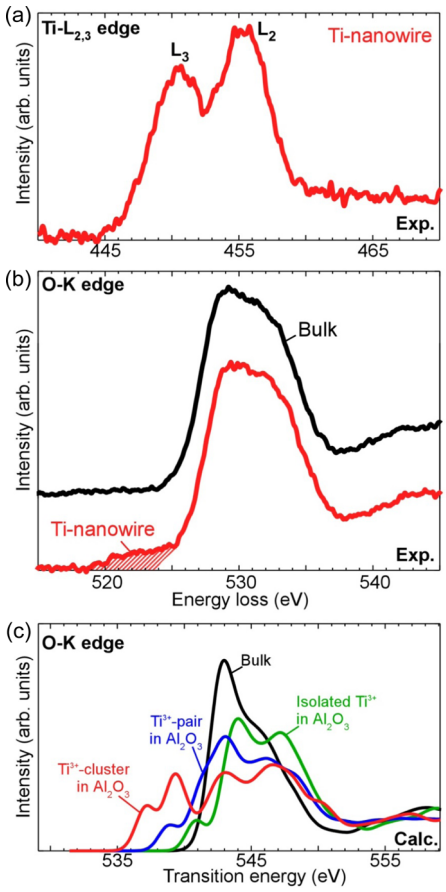


**Figure 6. Experimental and theoretical ELNES spectra, revealing the electronic structure within the nanowire fabricated in this study. (a) Experimental Ti $L_{2,3}$ ELNES spectrum, showing two separated peaks similar to those observed for $Ti_2O_3$. (b) Experimental O−K ELNES spectrum, showing a prepeak. (c) Theoretical O−K ELNES spectra based on first-principles DFT calculations. Collectively, these spectra show that a prepeak cannot result from isolated $Ti^{3+}$ ions in $Al_2O_3$ (as observed in (b)) but can result from $Ti^{3+}$ clusters. Thus, $Ti^{3+}$ ions concentrate along the dislocation line, and $Ti^{3+}$ clusters form in the conductive nanowire.**

with the extraordinarily hard surface of sapphire during conductivity measurements. In contrast, for nanowires at a 0.3° grain boundary, we were able to discriminate conduction by individual nanowires (Figure 5d). The interval of the electrical current peaks corresponds to the periodicity of the nanowire, suggesting that each nanowire contributes to the electric conduction. Conductivity reaches above 20 nA at each nanowire and is slightly higher than in Figure 5b, presumably because of variations in specimen thickness. Here notice that the electric conduction is brought about inside the insulating sapphire specimens with a thickness of several micrometers, each of which is sandwiched by evaporated metallic Au film and a Pt-coated Si cantilever probe with an applied voltage, as well as in the former report.[9]

To determine the mechanism of electric conductivity, we investigated the electronic structure of Ti in the nanowires by electron energy loss near-edge structures (ELNES) spectroscopy. Figure 6a,b shows experimental

and theoretical spectra of the Ti nanowire, respectively. The Ti $L_{2,3}$ ELNES spectrum (Figure 6a) shows two prominent peaks, similar to the case for $Ti_2O_3$.[27] This indicates that the valence state of Ti inside the nanowire is trivalent ($Ti^{3+}$), which is consistent with the results of former theoretical calculations[28−30] and shows that most of the Ti in $Al_2O_3$ becomes $Ti^{3+}$ ion under a heavy reducing atmosphere. The O−K ELNES spectrum (Figure 6b) shows a prepeak that is shaded in the figure, which is absent in the spectrum of bulk $Al_2O_3$.

To understand these ELNES results, we performed first-principles density functional theory (DFT) calculations of O−K ELNES spectra (Figure 6c) by the first-principles orthogonalized linear combination of atomic orbitals (OLCAO) method.[31] We calculated the ELNES spectra by constructing Ti-doped supercells composed of 120 atoms and introducing a core hole to an oxygen 1s orbital.[32] We then performed structure optimization around Ti by the first-principles projector-augmented wave (PAW) method.[33] The calculated spectra suggest that dilute and isolated $Ti^{3+}$ in bulk $Al_2O_3$ cannot form a significant prepeak, as we observed experimentally. However, a prepeak does appear when $Ti^{3+}$ forms a particular type of cluster. This finding is consistent with a previous theoretical prediction that $Ti^{3+}$ tends to form clusters in $Al_2O_3$.[29] That is, a number of $Ti^{3+}$ ions approach the dislocation line and form $Ti^{3+}$ clusters, which are present to a significant extent in the conductive nanowire. The electronic structure of $Ti^{3+}$ is $[Ar](3d)^1(4s)^0$, with the 3d electron available to contribute to electronic conduction. In fact, $Ti_2O_3$ that contains $Ti^{3+}$ ions is known to exhibit electronic conductivity to the point of being classified as a semiconductor. Thus, we conclude that the conductivity of the present nanowire is caused by the presence of $Ti^{3+}$ ions segregating along the dislocation line.

Unfortunately, a current−voltage graph at a nanowire was not able to be obtained in the present SPM measurements, although it is very useful in deeper discussion on the conduction mechanism if available. This is because a SPM probe is damaged by contact with the hard surface of sapphire during conductivity measurements as mentioned above. We think that the current−voltage graph from a nanowire is a future consideration.

## CONCLUSION

We successfully fabricated ordered, conductive nanowire arrays with periodicities of 13 or 90 nm inside insulating alumina oxide crystals, with array periodicity precisely controllable on a nanometer scale, by using periodic dislocations at crystal interfaces. This new fabrication method can be applied to any other crystalline material and is therefore a universal method for fabricating a periodic nanowire array inside a bulk crystal. It should therefore be widely applicable to the development of new electrical, magnetic, and optical devices.

## EXPERIMENTAL SECTION

**Microscopy.** The distribution of dislocations was investigated by conventional TEM (c-TEM; JEOL JEM-2010HC). The composition and chemical bonding state around the dislocations were analyzed by scanning TEM (STEM; JEOL JEM-2100F), energy-dispersive X-ray spectroscopy (EDS), and electron energy loss spectroscopy (EELS). The conductivity of the periodic nanowires was investigated by scanning probe microscope (SPM; JEOL JSPM-5200) in contact-current mode. Before SPM measurements, thin specimens were prepared by mechanical grinding and ion milling, in a similar manner followed for preparing TEM samples. For conductivity measurements, metallic Au was evaporated on one surface of a specimen, and then a Pt-coated Si cantilever probe with an applied voltage was allowed to contact the other surface.

*Conflict of Interest:* The authors declare no competing financial interest.

*Acknowledgment.* We thank Dr. E. Tochigi, Dr. J. P. Buban, Mr. E. Uehara, Mr. M. Tamura, and Mr. J. Tohma for their valuable discussions. This work was supported by a Grant-in-Aid for Scientific Research (A) (No. 22246088) and a Grant-in-Aid for Young Scientists (A) (No. 24686073, 22686059) from Japan Society for the Promotion of Science (JSPS).

## REFERENCES AND NOTES

1. Barnett, R. N.; Landman, U. Cluster-Derived Structures and Conductance Fluctuations in Nanowires. *Nature* **1997**, *387*, 788–791.
2. Nadj-Perge, S.; Frolov, S. M.; Bakkers, E. P. A. M.; Kouwenhoven, L. P. Spin-Orbit Qubit in a Semiconductor Nanowire. *Nature* **2010**, *468*, 1084–1087.
3. Peyrade, J. P.; Voillot, F.; Goiran, M.; Atmani, H.; Rocher, A.; Bedel, E. Atomic Scale Saw by Dislocation Slipping: A New Method To Generate One-Dimensional Structure. *Appl. Phys. Lett.* **1992**, *60*, 2481–2483.
4. Van Dam, J. A.; Nazarov, Y. V.; Bakkers, E. P. A. M.; De Franceschi, S.; Kouwenhoven, L. P. Supercurrent Reversal in Quantum Dots. *Nature* **2006**, *442*, 667–670.
5. Shockley, W. Dislocations and Edge States in the Diamond Crystal Structure. *Phys. Rev.* **1953**, *91*, 228.
6. Celli, V.; Gold, A.; Thomson, R. Electronic States on Dislocations in Semiconductors. *Phys. Rev. Lett.* **1962**, *8*, 96–97.
7. Hutson, A. R. Role of Dislocations in the Electrical Conductivity of CdS. *Phys. Rev. Lett.* **1981**, *46*, 1159–1162.
8. Fukuyama, H. Excitonic Superconductivity along Dislocations. *J. Phys. Soc. Jpn.* **1982**, *51*, 1709–1710.
9. Nakamura, A.; Matsunaga, K.; Tohma, J.; Yamamoto, T.; Ikuhara, Y. Conducting Nanowires in Insulating Ceramics. *Nat. Mater.* **2003**, *2*, 453–456.
10. Szot, K.; Speier, W.; Bihlmayer, G.; Waser, R. Switching the Electrical Resistance of Individual Dislocations in Single-Crystalline $SrTiO_3$. *Nat. Mater.* **2006**, *5*, 312–320.
11. Ran, Y.; Zhang, Y.; Vishwanath, A. One-Dimensional Topologically Protected Modes in Topological Insulators with Lattice Dislocations. *Nat. Phys.* **2009**, *5*, 298–303.
12. Ikuhara, Y. Nanowire Design by Dislocation Technology. *Prog. Mater. Sci.* **2009**, *54*, 770–791.
13. Wang, Z. C.; Tsukimoto, S.; Saito, M.; Ikuhara, Y. Individual Charge-Trapping Dislocations in an Ionic Insulator. *Appl. Phys. Lett.* **2009**, *95*, 184101.
14. Tokumoto, Y.; Amma, S.; Shibata, N.; Mizoguchi, T.; Edagawa, K.; Yamamoto, T.; Ikuhara, Y. Fabrication of Electrically

Conductive Nanowires Using High-Density Dislocations in AlN Thin Films. *J. Appl. Phys.* **2009**, *106*, 124307.
15. Amma, S.; Tokumoto, Y.; Edagawa, K.; Shibata, N.; Mizoguchi, T.; Yamamoto, T.; Ikuhara, Y. Electrical Current Flow at Conductive Nanowires Formed in GaN Thin Films by a Dislocation Template Technique. *Appl. Phys. Lett.* **2010**, *96*, 193109.
16. Shibata, N.; Chisholm, M. F.; Nakamura, A.; Pennycook, S. J.; Yamamoto, T.; Ikuhara, Y. Nonstoichiometric Dislocation Cores in α-Alumina. *Science* **2007**, *316*, 82–85.
17. Lagerlof, K. P. D.; Castaing, J.; Heuer, A. H. Do Moving Basal Dislocations in Sapphire ($\alpha$-$Al_2O_3$) Have Non-stoichiometric Cores?. *Philos. Mag.* **2009**, *89*, 489–499.
18. Cottrell, A. H.; Jaswon, M. A. Distribution of Solute Atoms Round a Slow Dislocation. *Proc. R. Soc. London, Ser. A* **1949**, *199*, 104–114.
19. Blavette, D.; Cadel, E.; Fraczkiewicz, A.; Menand, A. Three-Dimensional Atomic-Scale Imaging of Impurity Segregation to Line Defect. *Science* **1999**, *286*, 2317–2319.
20. Nakamura, A.; Lagerlof, K. P. D.; Matsunaga, K.; Tohma, J.; Yamamoto, T.; Ikuhara, Y. Control of Dislocation Configuration in Sapphire. *Acta Mater.* **2005**, *53*, 455–462.
21. Frank, F. C. Crystal Dislocations—Elementary Concepts and Definitions. *Philos. Mag.* **1951**, *42*, 809–819.
22. Lagerlöf, K. P. D.; Mitchell, T. E.; Heuer, A. H. Energetics of the Break-up of Dislocation Dipoles into Prismatic Loops. *Acta Metallogr.* **1989**, *37*, 3315–3325.
23. Bilde-Sørensen, J. B.; Lawlor, B. F.; Geipel, T.; Pirouz, P.; Heuer, A. H.; Lagerlöf, K. P. D. On Basal Slip and Basal Twinning in Sapphire ($\alpha$-$Al_2O_3$) - I. Basal Slip Revisited. *Acta Mater.* **1996**, *44*, 2145–2152.
24. Nakamura, A.; Yamamoto, T.; Ikuhara, Y. Direct Observation of Basal Dislocation in Sapphire by HRTEM. *Acta Mater.* **2002**, *50*, 101–108.
25. Heuer, A. H.; Jia, C. L.; Lagerlöf, K. P. D. The Core Structure of Basal Dislocations in Deformed Sapphire ($\alpha$-$Al_2O_3$). *Science* **2010**, *330*, 1227–1231.
26. Nakamura, A.; Matsunaga, K.; Yamamoto, T.; Ikuhara, Y. Multiple Dissociation of Grain Boundary Dislocations in Alumina Ceramics. *Philos. Mag.* **2006**, *86*, 4657–4666.
27. Lusvardi, V. S.; Barteau, M. A.; Chen, J. G.; Eng, J.; Fruhberger, B.; Teplyakov, A. An NEXAFS Investigation of the Reduction and Reoxidation of $TiO_2$ (001). *Surf. Sci.* **1998**, *397*, 237–250.
28. Matsunaga, K.; Nakamura, A.; Yamamoto, T.; Ikuhara, Y. First-Principles Study of Defect Energetics in Titanium-Doped Alumina. *Phys. Rev. B* **2003**, *68*, 214102.
29. Matsunaga, K.; Mizoguchi, T.; Nakamura, A.; Yamamoto, T.; Ikuhara, Y. Formation of Titanium-Solute Clusters in Alumina: A First-Principles Study. *Appl. Phys. Lett.* **2004**, *84*, 4795–4797.
30. Mizoguchi, T.; Sakurai, M.; Nakamura, A.; Matsunaga, K.; Tanaka, I.; Yamamoto, T.; Ikuhara, Y. Valence State of Ti in Conductive Nanowires in Sapphire. *Phys. Rev. B* **2004**, *70*, 153101.
31. Ching, W. Y.; Rulis, P. X-ray Absorption near Edge Structure/Electron Energy Loss near Edge Structure Calculation Using the Supercell Orthogonalized Linear Combination of Atomic Orbitals Method. *J. Phys.: Condens. Matter* **2009**, *21*, 104202.
32. Mizoguchi, T.; Olovsson, W.; Ikeno, H.; Tanaka, I. Theoretical ELNES Using One-Particle and Multi-Particle Calculations. *Micron* **2010**, *41*, 695–709.
33. Kresse, G.; Hafner, J. *Ab Initio* Molecular Dynamics for Open-Shell Transition Metals. *Phys. Rev. B* **1993**, *48*, 13115–13118.